

---

## Supporting Information:

# The Development of an Organic Lateral Resolution Test Device for Imaging Mass Spectrometry (IMS)

Melissa K. Passarelli,<sup>a,b,†,\*</sup> Jun Wang,<sup>a,b</sup> Amir Saeid Mohammadi,<sup>b</sup> Raphaël Trouillon,<sup>a</sup> Ian Gilmore<sup>c</sup> and Andrew G. Ewing<sup>a,b,\*</sup>

An organic lateral resolution test device has been developed to measure the performance of imaging mass spectrometry (IMS) systems. The device contains periodic gratings of polyethylene glycol (PEG) and lipid bars covering a wide range of spatial frequencies. Microfabrication technologies were employed to produce well-defined chemical interfaces, which allow lateral resolution to be assessed using the edge-spread function (ESF). In addition, the design of the device allows for the direct measurement of the modulation transfer function (MTF) to assess image quality. Scanning electron microscopy (SEM) and time-of-flight secondary ion mass spectrometry (ToF-SIMS) were used to characterize the device. ToF-SIMS imaging was used to measure the chemical displacement of biomolecules in MALDI matrix crystals. In a proof-of-concept experiment, the platform was also used to evaluate MALDI matrix application methods, specifically aerosol spray and sublimation methods.

In this file of Supporting Information, we provide additional details on

- the calculations describing the different spread functions obtained from an imaging system; **SI-1.**
- the specific case of an ESF for a Gaussian profile; **SI-2.**
- the liposome preparation; **SI-3.**
- the matrix deposition; **SI-4.**
- the characterization of device; **SI-5.**
- the use of the modulation transfer function (MTF) to assess the resolution of the system; **SI-6.**
- the characterization of matrix crystals using the device; **SI-7.**
- the data processing procedures to measure the lateral displacement of analytes in the system; **SI-8.**

---

*a* Department of Chemistry and Molecular Biology, University of Gothenburg, SE-405 30 Gothenburg, Sweden

*c* National Centre of Excellence in Mass Spectrometry Imaging (NiCE-MSI), National Physical Laboratory (NPL), Teddington, Middlesex, TW11 0LW, U.K.

*b* Department of Chemistry, Chalmers University of Technology, SE-412 96, Gothenburg, Sweden

\* Corresponding authors: melissa.passarelli@gmail.com, andrewewe@chalmers.se

\* present address: National Centre of Excellence in Mass Spectrometry Imag-

### SI-1: Lateral resolution measurement.

This section discusses the mathematical analysis of image resolution. During imaging, the final image  $i(x,y)$  is obtained from the initial object  $o(x,y)$  via the convolution with the im-

---

ing (NiCE-MSI), National Physical Laboratory (NPL), Teddington, Middlesex, TW11 0LW, U.K., melissa.passarelli@npl.co.uk

pulse function of the imaging system  $h(x,y)$ <sup>1</sup>

$$i(x,y) = [h * o](x,y) \quad (S1)$$

The quality of the imaging system is therefore largely dependent on the specificities of  $h$ . In the specific case of an optical system,  $h$  is the point spread function (PSF), *i.e.* the image obtained when the imaged object is a point (see Figure S1). This can be obtained trivially from Equation S1 by replacing the object function  $o(x,y)$  by a 2-dimensional Dirac delta function,  $\delta(x,y)$ , which is also the unit element for the convolution product

$$PSF(x,y) = [h * \delta](x,y) = h(x,y) \quad (S2)$$

Imaging a single point, therefore, provides valuable informations about the amount of blurring in the system. Although the mathematical function assumes an infinitesimally small point, the PSF is often approximated by a small disk. If the radius of the disk is too small to be finely resolved by the system, this is particularly relevant when the pixel size is on the same order of magnitude or larger than the disk radius, the PSF cannot be assessed.

We can reduce the constraints of the represented object function by integrating a point along a single axis to produce a line. In this case, the line spread function (LSF) can be obtained from Equation S1 by replacing the object function  $o(x,y)$  with a 1-dimensional Dirac pulse  $\delta(x)$ , instead of the 2-dimensional Dirac pulse  $\delta(x,y)$  required for the PSF.

$$\begin{aligned} LSF(x,y) &= [h * \delta](x,y) \\ &= \int \int h(x',y') \delta(x-x') dx' dy' \\ &= \int h(x,y') dy' \end{aligned} \quad (S3)$$

And from Equation S2

$$LSF(x) = \int_{-\infty}^{\infty} PSF(x,y') dy' \quad (S4)$$

Unfortunately, like the PSF, the LSF can also be hard to obtain experimentally. Again, the constraints of the represented object function can be reduced by integrating the line along its orthogonal axis to produce an edge. The edge spread function (ESF) the preferred method is obtained by imaging the edge of step function,  $s$

$$\begin{aligned} s(x) &= 0 \text{ if } x < 0, \\ &= 1 \text{ if } x \geq 0 \end{aligned} \quad (S5)$$

Immediately, using the properties of convolution for the inte-

gral of a function

$$\begin{aligned} ESF(x) &= \int_{-\infty}^{\infty} [h * s](x,y) dy \\ &= \int_{-\infty}^{\infty} [PSF * s](x,y) dy \\ &= \int_{-\infty}^x \int_{-\infty}^{\infty} [PSF * \delta](x',y) dx' dy \\ &= \int_{-\infty}^x LSF(x') dx' \end{aligned} \quad (S6)$$

Hence, acquiring the ESF from a simple object allows for the computing of the LSF, as summarized on Figure S1, and therefore to obtain fine details on the capabilities of the imaging system.

## SI-2: Measuring lateral resolution in SIMS imaging.

Lateral resolution in SIMS is typically measured using the edge-spread function (ESF), the function that describes the image convolution at a sharp edge. Several reports have suggested that a 2-dimensional Gaussian is a good approximation of the beam profile  $b(x,y)$

$$b(x,y) = A e^{-\frac{x^2+y^2}{2\sigma^2}} \quad (S7)$$

where  $A$  is a normalization constant.

Thanks to this approximation, it is possible to use the ESF to obtain the beam width  $\sigma$ . Assuming a Gaussian shaped beam, it has been demonstrated that the width of the rising section of the ESF is proportional to  $\sigma$ .<sup>2</sup> In this case, using the convolution shown on Equation S2 and S3, the image profile is proportional to the error function

$$\begin{aligned} ESF(x) &= \int_{-\infty}^x LSF(x') dx' \\ &\propto \int_{-\infty}^x \int_{-\infty}^{\infty} e^{-\frac{x'^2+y'^2}{2\sigma^2}} dx' dy' \\ &\propto \int_{-\infty}^x e^{-\frac{x'^2}{2\sigma^2}} dx' \\ &\propto erf\left(\frac{x}{\sigma\sqrt{2}}\right) + 1 \end{aligned} \quad (S8)$$

## SI-3: Liposome preparation.

All the glassware was rinsed in a 2 % solution of Deconex, then soaked in fresh 2 % solution of Deconex for 10 min at 70 °C, washed 5 times in deionized water and baked at 100 °C for 2 h.

Multi-lamellar liposomes were prepared with 1,2-dipalmitoyl-sn-glycero-3-phosphocholine [PC(16:0/16:0)]

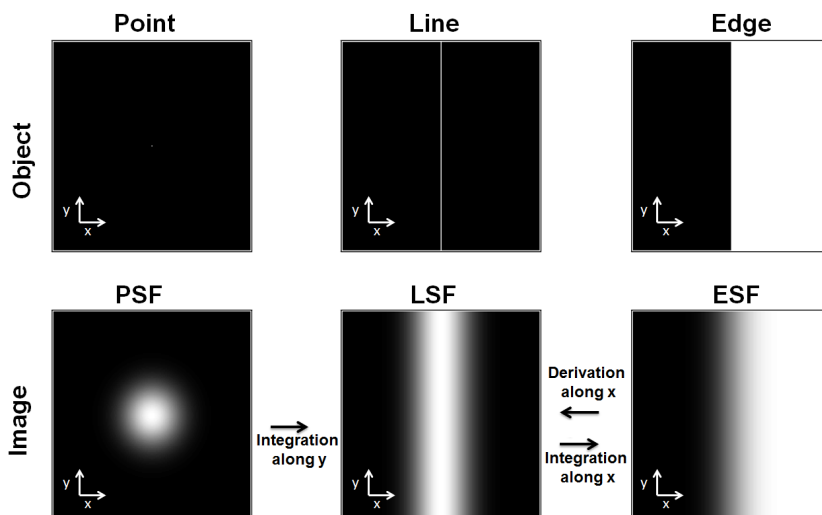


**Figure S1** The mathematical relationship between the point spread function (PSF), the line spread function (LSF) and the edge spread function (ESF) are represented pictorially. The diagram demonstrates the convolution or blurring of feature such a point, a line and an edge by a imaging system with a Gaussian beam profile. The top row shows the real or virtual target objects and the bottom row contains the corresponding images.

and cholesterol (Avanti Polar Lipids, USA). A 5 mL solution containing a 80:20 mixture of PC(16:0/16:0) and cholesterol in chloroform was rotovaped for one hour. The solution was rehydrated in 5 mL of deionized water for 30 min. The solution was placed in a  $-80\text{ }^{\circ}\text{C}$  freezer until frozen, then immediately thawed. The freeze/thaw cycle was repeated 5-time. Approximately, 1 mL of the liposome solution was deposited on the PEG functionalized test device. The solution was agitated with a pipette and left to incubate for 10 min. The liposome solution was removed and the test device was washed 5 times with deionized water and dried with nitrogen gas.

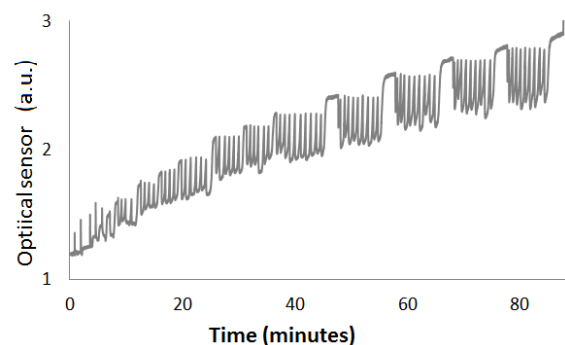


**Figure S2** The controlled deposition of the matrix on the device is shown, the optical sensor voltage is plotted as a function of time.

#### SI-4: Matrix deposition.

MALDI matrix was applied to the device with a Bruker ImagePrep sprayer (Bremen, Germany) and the standard spray method for 2,5-dihydroxybenzoic acid (DHB) matrix was used. The recording from the sprayer's optical sensor, tracking the deposition process, is shown in Figure S2

For solvent free matrix deposition, DHB was applied to the device using a sublimation apparatus (Sigma-Aldrich). Under vacuum, the device was cooled to about  $4\text{ }^{\circ}\text{C}$  with recirculating ice water and a reservoir containing DHB matrix was heated to  $220\text{ }^{\circ}\text{C}$  using a sandbath. The DHB matrix was deposited on the device for approximately 20 minutes.

#### SI-5: Characterization of the device.

ToF-SIMS was used to characterize the device. The ion image in Figure 3B of the main text, shows the chemical distribution of lipid and PEG on the device and the monochromatic images for each of the color channel in the RGB image are displayed in Figure S3. The FWHM measured from linescans obtained from this image, as well as, other images are displayed in Table S1. In addition, the falling edge of the PEG ( $m/z$  107 only) was fitted to the error function and the parameter  $\sigma$  was measured for each bar in the image (see Table S2).

**Table S1** The measured full-width at half-maximum (FWHM) for the device obtained from the SEM and ToF-SIMS images of the unfunctionalized test device and ToF-SIMS image obtained from the functionalized test device.

Expected ( $\mu\text{m}$ )	SEM		ToF-SIMS (unfunc.)		ToF-SIMS (func.)	
	$\text{SiO}_2$ ( $\mu\text{m}$ )	Gold ( $\mu\text{m}$ )	$\text{SiO}_2$ ( $\mu\text{m}$ )	Gold ( $\mu\text{m}$ )	Lipid ( $\mu\text{m}$ )	PEG ( $\mu\text{m}$ )
3.0	3.0	–	2.8	–	2.8	–
4.0	3.6	4.2	4.2	4.2	3.8	3.8
5.0	4.8	4.8	5.6	5.2	4.7	4.7
6.0	6.0	6.0	6.3	6.3	5.6	5.6
7.0	7.2	7.2	7.3	7.0	7.5	6.6
8.0	7.8	8.4	8.7	–	8.4	7.5
9.0	9.0	9.0	–	–	9.4	8.5
10.0	9.6	10.2	–	–	10.4	9.4
10.0	9.6	10.8	–	–	10.4	9.4
20.0	19.8	20.4	–	–	20.7	19.8
30.0	30.0	30.6	–	–	–	29.2
40.0	40.8	40.2	–	–	–	–
50.0	51.0	–	–	–	–	–

**Table S2** The falling edges in the PEG ( $m/z$  107) linescans, corresponding to the ESF of the IMS system, were fit to the sigmoidal curves. The fitting parameters, described in the main text, were used to calculate the  $\Delta_{88\%-12\%}$  which is equal to the *FWHM* of the Gaussian beam.

Bar width ( $\mu\text{m}$ )	$\sigma$ ( $\mu\text{m}$ )	$X_{88\%}$ ( $\mu\text{m}$ )	$X_{12\%}$ ( $\mu\text{m}$ )	$\Delta_{88\%-12\%}$ ( $\mu\text{m}$ )
4.0	0.79	51.63	49.77	1.86
5.0	1.15	61.02	58.32	2.70
6.0	0.74	71.58	69.85	1.73
7.0	0.55	84.48	83.20	1.28
8.0	0.54	99.38	98.11	1.27
9.0	0.62	116.38	114.93	1.46
10.0	0.64	135.31	133.82	1.49
20.0	0.53	184.91	183.67	1.24
30.0	0.60	234.64	233.24	1.40
Average				1.45
St. Dev.				0.64

## SI-6: The modulation transfer function MTF.

The ability to resolve features and contrast are strongly linked to the spatial frequency of the object. It is therefore informative to take the Fourier transform of Equation S1

$$\begin{aligned}
 \mathcal{F}(i)(f, g) &= \mathcal{F}(h * o)(f, g) \\
 &= \mathcal{F}(h)(f, g) \mathcal{F}(o)(f, g) \\
 &= \mathcal{F}(PSF)(f, g) \mathcal{F}(o)(f, g)
 \end{aligned} \tag{S9}$$

where the operator  $\mathcal{F}$  indicates the Fourier transform,  $f$  and  $g$  being the variables of the 2-dimensional frequency space. In this representation,  $\mathcal{F}(h)$  can be seen as a function transfer giving the final image from the object. By definition, the

modulation transfer function (MTF) is obtained from  $\mathcal{F}(h)$

$$MTF(f, g) = |\mathcal{F}(PSF)(f, g)| \tag{S10}$$

As summarized in Equation S11, the MTF can be numerically obtained from the Fourier transform of the PSF, which in 1 dimension is equivalent to taking the Fourier transform of the LSF. In our Gaussian profile approximation, the profile of the LSF is proportional to a Gaussian. Using the properties of the Fourier transform of a Gaussian, we can then write that

$$\begin{aligned}
 MTF(f) &= |\mathcal{F}(LSF)(f)| \\
 &\propto \left| \mathcal{F}\left(e^{-\frac{x^2}{2\sigma^2}}\right)(f) \right| \\
 &\propto e^{-2\pi^2 \sigma^2 f^2}
 \end{aligned} \tag{S11}$$

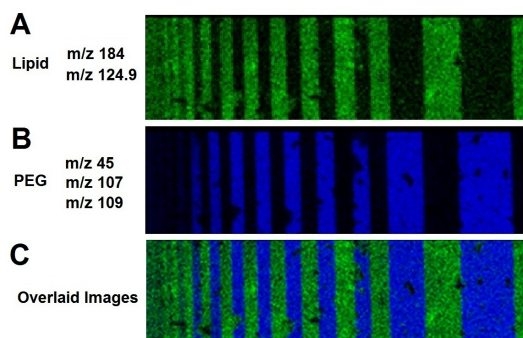


**Figure S3** A) The sum of the lipid peaks at  $m/z$  184 and 124.9 are displayed in green. B) The sum of the PEG peaks at  $m/z$  45, 107, and 109 are displayed in blue. C) The combined images from A and B show that the lipid and PEG regions are anti-colocalized.

From this expression, we can calculate  $f_{50\%}$ , the frequency corresponding to half the maximal MTF value:

$$f_{50\%} = \frac{\sqrt{\ln(2)}}{\pi\sigma\sqrt{2}} \quad (\text{S12})$$

### SI-7: The characterization of matrix crystals using the device.

The chemical distribution of matrix crystals on the device is shown in Figure 5 of the main text. The monochromatic images that combine to form the RGB image are displayed in Figure S4. Matrix-related peaks at  $m/z$  136, 137, 154, and 155, lipid-related peaks at  $m/z$  184 and 124.9, and PEG-related peaks at  $m/z$  45, 107, and 109 are summed to form the red, green and blue monochromatic images, respectively.

In order to isolate individual matrix crystals from the image, MATLAB software was used to produce a masks for each of the selected crystals. The summed contribution of all ten masks overlaid together is shown in Figure S4. When the mask is applied to the RGB image, the complicated background is eliminated and the chemical mixing within individual matrix crystals is elucidated.

Basic geometric measurements of the selected matrix crystal are displayed in Table S3. The length and width of the individual crystals were measured with ImageJ software (details in Figure S4). The area was calculated in MATLAB software, simply by multiplying the pixel area by the number of pixels in the single crystal mask.

The mask was applied to the individual ion images and the secondary ion intensity per crystals area was calculated for each crystal, the average and standard deviation for each measurement is provide in Table S4. The percent coverage was calculated by taking the ratio of pixels containing signal from that particular mass peak compared to the total number of pix-

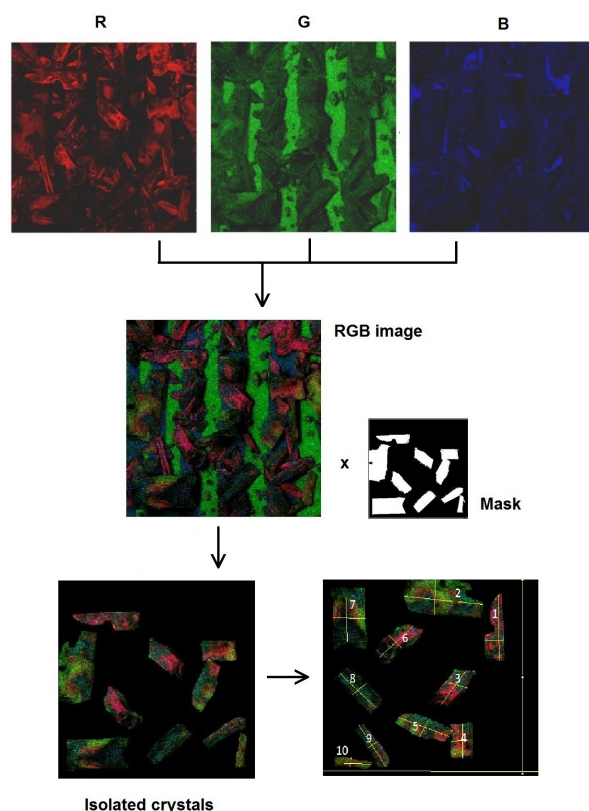


**Figure S4** Diagram of the data processing workflow for characterizing individual matrix crystal from an ToF-SIMS ion image. Monochromatic images of the matrix (red), lipid (green) and PEG (blue) are combined to make an RGB image, a digital mask is applied to the image in order to isolate specific features for characterization.

els in the crystal. Again this value was calculated for each matrix crystal and the average and standard deviation are compiled in Table S4.

### SI-8: Lateral displacement of analytes in the matrix crystal.

The lateral migration of analytes in a single matrix crystal was assessed by measuring the distance between the pixel in which the chemical was detected and the chemical interface. The data processing workflow is provided in Figure S5. In MATLAB, a single crystal was extracted from the ion image using a mask, as described in the previous section. Based on the location of the PEG-lipid interfaces, the pixels were given new  $x$ ,  $y$  coordinates and the data was divided along the center of the PEG bar. The lipid molecules migrating into the PEG region of the device and vice-versa are mapped, for both the left-hand side and right hand side of the PEG bar. The migration distance is estimated to be roughly the

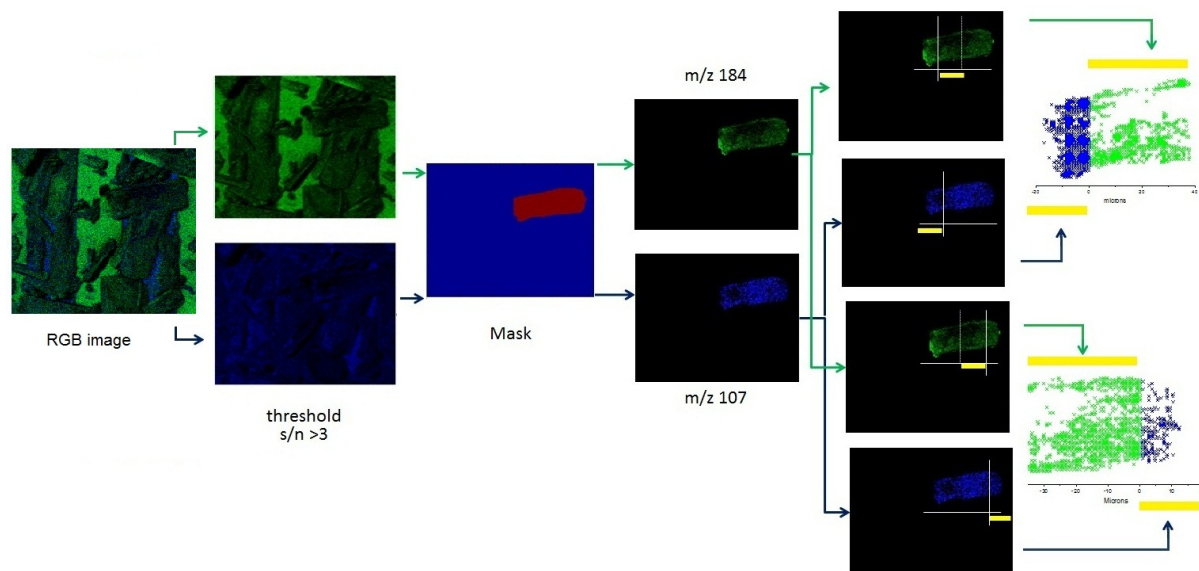


**Figure S5** Data processing workflow for assessing analyte migration in a single matrix crystal grown on the device. In the ToF-SIMS ion image lipid is represented by the peak at  $m/z$  184 (green) and PEG by the peak at  $m/z$  107 (blue). A digital mask was applied to the individual monochromatic ion images to isolate the single matrix pixel. New axes were assigned based on the location of the PEG-lipid interfaces. The distance between a pixel with detectable quantity of analyte and the interface was calculated and used to describe mobility.

**Table S3** The length, width and area for the labeled DHB matrix crystals in Figure 5 (and Figure S4) were measured and the average crystal dimensions were calculated.

Crystal number	Width ( $\mu\text{m}$ )	Length ( $\mu\text{m}$ )	Area ( $\mu\text{m}^2$ )
1	43	170	85.5
2	91	182	129.4
3	52	104	73.5
4	48	88	65.0
5	51	125	80
6	42	114	69
7	75	138	101
8	43	121	72
9	27	122	57.4
10	22	83	72.7
Average	49.4	124.7	77.6

distance of the pixel with respect to the interface. Although a number of factors influence the measurement (*i.e.* crystal size, orientation, nucleation site, matrix chemistry, analyte chemistry and thresholding), the proof-of-concept experiment shows that analyte migration can be assessed by combining ToF-SIMS imaging and the described patterned surface.

**Table S4** The chemical characteristics of the ten isolated matrix crystals imaged in Figure 5 (and Figure S4). The average counts per  $\mu\text{m}^2$  and the percent coverage for the main chemical components –PEG, lipid and matrix–were calculated for each crystal.

	$m/z$	Ion Density Counts per $\mu\text{m}^2$		Coverage (%)	
		Average	St. Dev.	Average	St. Dev.
PEG	44	13.6	5.0	46.0	8.8
	107	5.7	2.0	21.9	7.0
Lipid	184	57.9	25.9	86.7	7.9
	125	15.1	6.2	49.5	9.5
Matrix	136	60.4	26.4	73.7	16.7
	137	129.9	51.4	87.5	11.6
	154	49.2	25.0	62.7	19.5
	155	63.3	30.3	69.5	18.4

**Contributions.** MKP: inception, designed the device, performed experiments, analyzed data, wrote the manuscript; JW: prepared the device, contributed to the design, wrote a portion of the microfabrication section; ASM: participated in early stages of the device design, suggested nanofabrication for device manufacturing; RT: contributed to the data analysis, established the theoretical framework, wrote portions of the theory, MTF and SI section; ISG: head of lab where the data

---

was processed and manuscript written, processing advice;  
AGE: head of the lab where the experiments were performed,  
provided environment, acquired funding.

## References

- 1 X. Zhang, T. Kashti, D. Kella, T. Frank, D. Shaked, R. Ulichney, M. Fischer and J. P. Allebach, *IS&T/SPIE J. Electron. Imaging*, 2012, pp. 829307–829307.
- 2 M. Seah, *Surf. Interface Anal.*, 2002, **33**, 950–953.